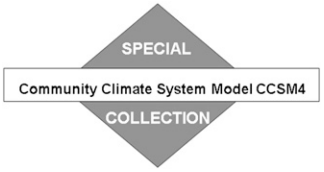

Wintertime Atmospheric Response to North Atlantic Ocean Circulation Variability in a Climate Model

CLAUDE FRANKIGNOUL AND GUILLAUME GASTINEAU

Sorbonne Universités, UPMC/CNRS/IRD/MNHN, LOCEAN/IPSL, Paris, France

YOUNG-OH KWON

Woods Hole Oceanographic Institution, Woods Hole, Massachusetts

(Manuscript received 30 December 2014, in final form 30 June 2015)

ABSTRACT

Maximum covariance analysis of a preindustrial control simulation of the NCAR Community Climate System Model, version 4 (CCSM4), shows that a barotropic signal in winter broadly resembling a negative phase of the North Atlantic Oscillation (NAO) follows an intensification of the Atlantic meridional overturning circulation (AMOC) by about 7 yr. The delay is due to the cyclonic propagation along the North Atlantic Current (NAC) and the subpolar gyre of a SST warming linked to a northward shift and intensification of the NAC, together with an increasing SST cooling linked to increasing southward advection of subpolar water along the western boundary and a southward shift of the Gulf Stream (GS). These changes result in a meridional SST dipole, which follows the AMOC intensification after 6 or 7 yr. The SST changes were initiated by the strengthening of the western subpolar gyre and by bottom torque at the crossover of the deep branches of the AMOC with the NAC on the western flank of the Mid-Atlantic Ridge and the GS near the Tail of the Grand Banks, respectively. The heat flux damping of the SST dipole shifts the region of maximum atmospheric transient eddy growth southward, leading to a negative NAO-like response. No significant atmospheric response is found to the Atlantic multidecadal oscillation (AMO), which is broadly realistic but shifted south and associated with a much weaker meridional SST gradient than the AMOC fingerprint. Nonetheless, the wintertime atmospheric response to the AMOC shows some similarity with the observed response to the AMO, suggesting that the ocean–atmosphere interactions are broadly realistic in CCSM4.

1. Introduction

The influence of oceanic variability on the large-scale atmospheric circulation is difficult to detect at extratropical latitudes, because the atmospheric response has limited amplitude and the internal variability of the atmosphere is large, in particular during the cold season, resulting in a small signal-to-noise ratio. However, as the intrinsic atmospheric persistence is short and the atmospheric noise decreases with increased averaging, the oceanic impact should be easier to detect, and more influential, at low frequency, provided that the surface heat flux anomalies that drive it be sufficiently persistent. Since sea surface temperature (SST) anomalies tend to be damped by the negative surface heat flux feedback (Frankignoul and Kestenare 2002; Park et al. 2005), persistent anomalous heating or cooling mostly reflects persistent SST anomalies. Although their persistence is larger at high latitudes in the cold season when the surface mixed layer is deep, and it may be enhanced by SST reemergence (Namias and Born 1970; Alexander and Deser 1995; de Coëtlogon and Frankignoul 2003), the largest sources of extratropical SST persistence are tropical forcing, which affects, in particular, the Pacific decadal oscillation (e.g., Schneider and Cornuelle 2005) and ocean circulation variability; the latter strongly contributes to the Atlantic multidecadal oscillation (AMO), at least in climate model simulations where it is driven by changes in the Atlantic meridional overturning circulation (AMOC)

Corresponding author address: Claude Frankignoul, University Pierre and Marie Curie, LOCEAN, 4 place Jussieu, 75252 Paris CEDEX 05, France.
E-mail: cf@locean-ipsl.upmc.fr

DOI: 10.1175/JCLI-D-15-0007.1

(e.g., Knight et al. 2005; Medhaug and Furevik 2011; Danabasoglu et al. 2012b; Marini and Frankignoul 2014). The AMO, which has a dominant period of about 70 yr, has been reported to have a large influence on summer temperature and precipitation, in particular in Europe and North America, and it may affect Atlantic hurricane activity (e.g., Enfield et al. 2001; Goldenberg et al. 2001; Sutton and Hodson 2005; Klotzbach 2011). In winter, the AMO was shown to drive a negative phase of the North Atlantic Oscillation (NAO) in models and observations, which promotes the occurrence of cold temperature events over North America and Europe (Ting et al. 2014; Peings and Magnusdottir 2014; Gastineau and Frankignoul 2015). Omrani et al. (2014) provided further modeling evidence that a warm phase of the AMO can drive a negative NAO. In addition, Gulev et al. (2013) showed that the AMO drives the observed surface heat fluxes at low frequency.

Since the observations are limited, to understand how the AMOC impacts the atmospheric circulation, one must rely on climate model simulations, most conveniently so by using control simulations where there is no need to distinguish the influence of the AMOC variability from that of external or anthropogenic forcing. AMOC's impact on the North Atlantic–European sector has been detected during the cold season in several climate models. Msadek et al. (2011) found a negative NAO response in winter to an AMOC intensification via its AMO-like SST footprint in a control simulation with the IPSL-CM4 climate model; Gastineau and Frankignoul (2012) showed that an AMOC intensification tends to be followed by a positive AMO and a negative NAO in six climate models, albeit with different time lags; and Gastineau et al. (2013) showed that the wintertime atmospheric response to AMOC variability in IPSL-CM5 was broadly consistent with the observed atmospheric response to North Atlantic SST anomalies. On the other hand, Frankignoul et al. (2013) found in the red-noise regime that characterizes the latter part of the CCSM3 control simulation that an AMOC intensification was rapidly followed by a positive NAO phase during winter, and they suggested that the difference with the models in Gastineau and Frankignoul (2012) was due to the SST signature of the AMOC being dominated in CCSM3 by the large meridional shifts of the Gulf Stream–North Atlantic Current (GS–NAC) that covaried with the AMOC. It is thus of interest to investigate the AMOC influence on the atmospheric circulation and its link with its time-evolving SST footprint and the GS–NAC variability in the NCAR Community Climate System Model, version 4 (CCSM4), which has many improved parameterizations in both the atmosphere and ocean and a more realistic representation of the AMO (Gent et al. 2011; Danabasoglu et al. 2012a,b). After briefly describing the coupled model (section 2), we use maximum covariance analysis (section 3) and lag regression to discuss the atmospheric forcing of the AMOC in section 4 and to detect the AMOC influence on the wintertime atmospheric circulation in section 5. The links between the AMOC variability, GS–NAC shifts, and the atmospheric response are discussed in section 6. Section 7 includes a summary, a brief comparison with the observations, and a discussion.

2. Model

The CCSM4 is described in Gent et al. (2011). Its components are the Community Atmosphere Model, version 4 (CAM4), with 26 vertical levels and nominal 1° resolution (1.25° × 0.9°); the Parallel Ocean Program, version 2 (POP2), with a nominal 1.11° zonal resolution and a 0.27° meridional resolution at the equator, gradually increasing to 0.54° at 33°N/S, and 60 levels in the vertical; the Community Land Model, version 4 (CLM4); and the Sea Ice Model, version 4 (CICE4). The control integration uses greenhouse gas concentrations set to their 1850 levels. It was run for 1300 yr without any flux adjustment, and we use the last 500 yr of the simulation, when the model drift is small and the AMOC has reached an approximately statistically steady state (Danabasoglu et al. 2012b).

The ocean model in CCSM4 uses a quadratic bottom drag and includes a parameterization of submesoscale eddy mixing and overflow parameterization, among various improvements from its predecessor CCSM3. The oceanic circulation has been described in Gent et al. (2011) and Danabasoglu et al. (2012a) and is only briefly discussed here. In general, the oceanic fields are realistic in the North Atlantic, and they show less bias than in CCSM3, with narrower boundary currents and a better representation of the Nordic Seas overflow. Although the cold bias in the North Atlantic found in CCSM3 has been reduced in CCSM4, the GS path (Fig. 1, top) remains too far north and only separates from the coast at about 43°N near the Tail of the Grand Banks and flows more or less zonally, while, in observations, the GS separates near Cape Hatteras (~35°N) and has a cyclonic northern recirculation gyre to the north (between the GS and the continental shelf) before abruptly turning northward near the Tail of the Grand Banks and turning again eastward near the Flemish Cap to form the Northwest Corner (~50°N, 44°W; Rossby 1996). These are typical deficiencies found in most climate models of similar resolution. Also, the NAC is too zonal and crosses the Mid-Atlantic Ridge south of the Charlie–Gibbs Fracture Zone/Faraday Fracture Zone. Hence, there is warm and salty bias along the North American coast and a cold and fresh bias along the observed NAC path. The main

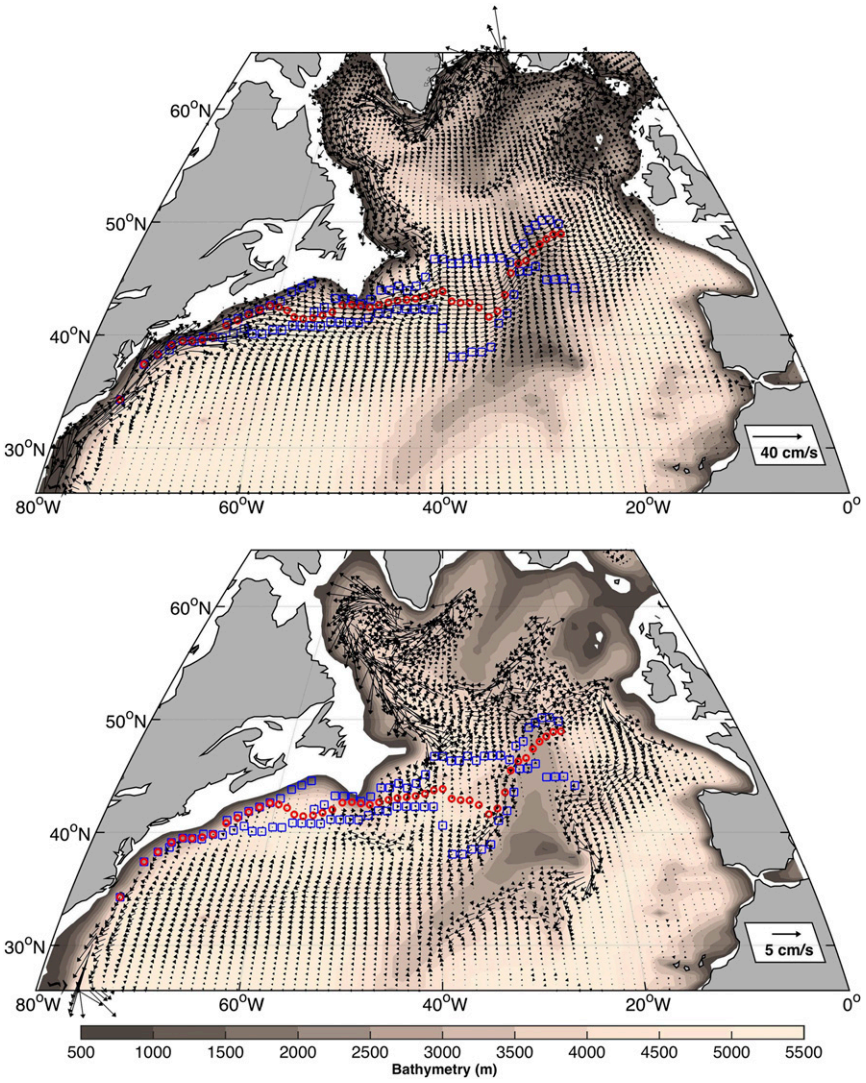

FIG. 1. Mean GS–NAC path, as defined by the latitude of maximum 0–500-m eastward velocity (red) and its most northern and southern position (blue) superimposed on the mean (top) 0–500-m and (bottom) 2000–3000-m velocity. Topography is given by shading.

deep convection sites are located in the central Labrador Sea, south of Cape Farewell, and in the Nordic Sea along the ice edge. The deep Atlantic is slightly too warm and salty. The deep circulation (2000–3000 m) exhibits a strong cyclonic boundary current in the subpolar gyre, but there is no well-defined deep western boundary current between the Flemish Cap and Cape Hatteras (Fig. 1, bottom). Instead, the deep equatorward flow detaches from the western boundary near Flemish Cap and follows an interior path along both flanks of the Mid-Atlantic Ridge, returning to the western boundary near and south of Cape Hatteras so that the crossover between the GS–NAC and the deep equatorward flow occurs near the western flank of the Mid-Atlantic Ridge. This interior pathway is similar to that suggested by recent observations and an eddy-resolving ocean model (Bower et al. 2009). Furthermore, there is an interaction between the southward boundary currents and eastward equivalent barotropic GS–NAC near the Tail of the Grand Banks. The mean AMOC is stronger than in CCSM3, reaching 26 Sv ($1\ \mathrm{Sv} = 10^6\ \mathrm{m^3\ s^{-1}}$), but its variability is reduced, with dominant low-frequency variability in the 50–100-yr range and large interannual variability. See Danabasoglu et al. (2012b) for more details and a discussion of the impacts of the parameterized Nordic Sea overflows onto the AMOC. The mean SST in the equatorial Pacific is well represented, although warmer than observed at the western and eastern boundaries, and the El Niño–Southern Oscillation (ENSO) has a rather realistic

period (3–6 yr) but too large an amplitude, with broadly realistic but exaggerated global teleconnections (Deser et al. 2012). This leads to a link between ENSO and the AMOC, as discussed below.

3. Statistical analysis

The main patterns of covariability between the ocean and the atmosphere are investigated with a lag maximum covariance analysis (MCA; Bretherton et al. 1992; Czaja and Frankignoul 2002), which isolates pairs of spatial patterns and their associated time series by performing a singular value decomposition of the area-weighted covariance matrix between two fields. Here, we primarily use 3-month running means of 500-hPa geopotential height (Z500) anomalies (mean seasonal cycle subtracted) in the North Atlantic sector (20°–80°N; 90°W–40°E) and, as oceanic fields, 12-month running means of the AMOC streamfunction between 30°S and 80°N or the meridional position of the GS–NAC, given by the maximum zonal velocity in the upper 500 m. To emphasize the low-frequency variability and increase the signal-to-noise ratio without affecting seasonality, we apply a binomial smoothing (¼–½–¼) to each seasonal atmospheric and yearly AMOC time series prior to the MCA, as well as to the GS–NAC metric, unless stated otherwise. For example, January–March (JFM) at year t, JFM_t, is replaced by $\frac{1}{4}\,\mathrm{JFM}_{t-1} + \frac{1}{2}\,\mathrm{JFM}_t + \frac{1}{4}\,\mathrm{JFM}_{t+1}$. To remove possible model drift, a second-order trend was removed from all variables prior to analysis. Each MCA mode is characterized by its squared covariance (SC), the correlation (R) between the two time series, and the SC fraction (SCF) that it represents. To establish whether the MCA modes are meaningful, statistical significance is estimated using a moving blocks bootstrap approach: each MCA was repeated 100 times, linking the original oceanic anomalies with randomly scrambled atmospheric fields based on 5-yr blocks to take into account the influence of possible serial correlation in the atmosphere. The quoted significance levels indicate the number of randomized SC and correlation R that exceeds the value being tested. A smaller significance level indicates stronger evidence against the null hypothesis (atmosphere and ocean are independent). When the ocean leads, we show homogeneous covariance maps (regression on the same field MCA time series) for the ocean and heterogeneous covariance maps (regression on the other field time series) for the atmosphere. When the atmosphere leads, we show homogeneous covariance maps for the atmosphere and heterogeneous covariance maps for the ocean. This preserves orthogonality (Czaja and Frankignoul 2002) and reflects the physics of the ocean–atmosphere interaction. The MCA time series were standardized; hence, the maps show typical amplitude.

In most cases, when the atmosphere leads or is simultaneous with the ocean, the MCA primarily reflects the atmospheric forcing of the ocean, while, when the ocean leads, it reflects the atmospheric response to the ocean. Because of the temporal smoothing, results at neighboring lags are not independent. However, the strong simultaneous relation between Z500 anomalies and the AMOC or the GS–NAC position, which reflects the ocean response to the atmosphere, only weakly biases the results when the oceanic variable leads by 2 yr (lag 2), and the results should only reflect the oceanic influence when the ocean leads by 3 yr or more (lag ≥ 3). Yet persistent tropical teleconnections may induce a lagged correlation between ocean and atmosphere that is not linked to an atmospheric response to the extratropical ocean. Hence, when (and only when) the ocean leads, we remove these teleconnections from both atmospheric and oceanic variables by multivariate regression, assuming that they are instantaneous in the atmosphere (which is reasonable for 3-month averages), while they vary with lag for the ocean in order to get unbiased estimates (see Frankignoul et al. 2011). This was also done for the lagged regressions. The tropical SST is represented by the first three principal components (PCs) of the 3-month running averages of SST anomalies between 12.5°S and 12.5°N in the tropical Pacific, and the regressions are done separately for positive and negative values of the PCs to take into account the asymmetry of the ENSO teleconnections. As they vary with the season, the regressions are performed separately for each season. The teleconnections with the tropical Indian and Atlantic Oceans were not removed, but it was verified that they had no impact on the atmospheric response discussed in section 4.

The same methodology is applied using Northern Hemisphere sea level pressure (SLP), Z500, and surface heat flux as atmospheric fields and AMOC as an oceanic field. Last, we also perform a similar MCA between Northern Hemisphere Z500 and North Pacific SST (between 20° and 60°N).

4. Atmospheric forcing of the AMOC

The MCA is first used to determine the main lead and lag relations between the AMOC and the large-scale atmospheric circulation as a function of season. The strongest covariability is found when the AMOC lags Z500 in fall, winter, and spring by about 2–3 yr, with maximum covariance when Z500 is in JFM (Fig. 2). In JFM [and December–February (DJF)], the SC and the R are 5% significant for lags between 0 and −8 (Z500

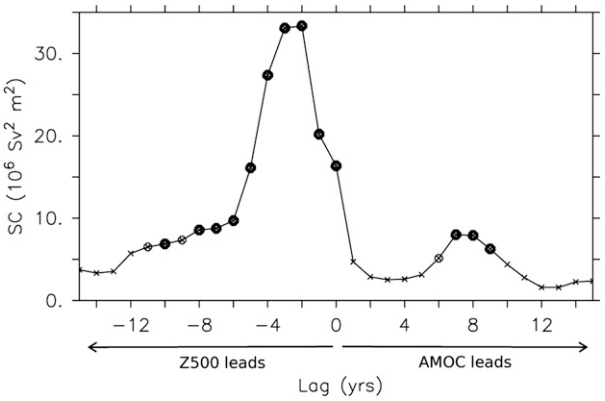

FIG. 2. Squared covariance (10^6 Sv^2 m^2) of the first MCA mode between Z500 in JFM and the AMOC streamfunction as a function of time lag (yr), with AMOC leading at positive lags. Full circles indicate 5% significance of the SC and open circles 10% significance.

leads), reflecting the forcing of the AMOC by the NAO during the cold season, a positive NAO leading an AMOC amplification. Note that the NAO in CCSM4 is biased, as discussed by Davini and Cagnazzo (2014): the northern center of action is almost centered on the Arctic, and the midlatitude centers of action are too separated, which produces a spatial pattern too annular. The wobbling of the eddy-driven jet that characterizes the NAO is very weak because the jet stream is displaced poleward, and thus the frequency of Greenland blocking is strongly underestimated.

As illustrated for lag −3 in Fig. 3 (top), the AMOC response is first limited to the North Atlantic. However, it can be shown that it progressively expands southward, extending throughout the whole basin by lag −8, which makes it more similar to the AMOC EOF-1 pattern [see Fig. 2 of Danabasoglu et al. (2012b), close to Fig. 4 below]. Similar results are obtained when using SLP instead of Z500, as expected from the barotropic structure of the NAO (Thompson et al. 2003). The MCA AMOC pattern has limited amplitude, however, reaching only about half of that of the AMOC EOF-1 pattern, which suggests that primarily stochastic NAO forcing only indirectly triggers the main mode of AMOC variability. Danabasoglu et al. (2012b) have shown that the AMOC variability is indeed largely driven by salinity-dominated density anomalies at the Labrador Sea deep-water convection site, which are, in part, controlled by surface fluxes and subpolar gyre circulation changes, and they speculated that the latter were set by the NAO. Hence, as in CCSM3 (Kwon and Frankignoul 2012), the direct NAO forcing of the AMOC is limited.

However, the Indo-Pacific also plays a role in driving the AMOC, presumably because ENSO in CCSM4 has too large an amplitude and exaggerated global teleconnections (Deser et al. 2012). This is shown in Fig. 3 by separate MCAs at lag −3 between the AMOC and JFM (second row) SLP, (third row) SST, and (bottom) surface heat flux, north of 10°S, which are all highly significant and show the same AMOC pattern, albeit with a slightly smaller amplitude. Similar results are found at lag −4, while in each case the first two MCA modes are poorly separated at lag −1 and −2 (not shown). The SST pattern shows a La Niña event in the equatorial Indo-Pacific, a strong signal in the North Pacific, and a weaker one in the Atlantic. A rather similar pattern is found for the heat flux, albeit with a stronger amplitude in the North Atlantic. Note the polarity of the heat flux, which is driven by SST in the tropical Indo-Pacific (the heat flux tends to damp SST anomalies, as in observations) but drives SST in the North Pacific and in the Atlantic (downward heat flux over warm SST), consistent with a Pacific–North American teleconnection pattern. In this model, the latter projects onto the Arctic Oscillation (Fig. 3, right column in second panels), which presumably explains how ENSO affects the AMOC. Li and Lau (2012) have shown that there is a similar, albeit weaker, relation between ENSO and the NAO in the observations, which was attributed to transient eddy effects. Similar results are obtained by limiting SST and the heat flux in the MCA to the Indo-Pacific, showing their robustness. However, as the SC remains significant at larger lead time with North Atlantic Z500 or SLP (5% significant for lag up to −9) than with SLP in the entire region north of 10°S (5% significant only for lag up to −5), the intrinsic NAO variability seems to dominate the AMOC forcing. There is no significant relation with the tropical Indo-Pacific SST or heat flux when the AMOC leads, so the interaction with the tropics is only one way. Note that the latitudes south of 10°S do not play a role in driving the AMOC variability (at least at lag ≥ -8 yr), as it is not associated with any significant SST or surface heat flux anomalies in the Southern Ocean. This is consistent with Yeager and Danabasoglu (2014), who found that late-twentieth-century interannual-to-decadal Atlantic circulation variability as simulated in an ocean–sea ice hindcast configuration of CCSM4 was almost entirely explained by subpolar forcing. It may reflect that the equator acts as a low-pass filter (buffering effect) for overturning circulation anomalies driven at high southern (or northern) latitudes (Johnson and Marshall 2002; see also Deshayes and Frankignoul 2005).

5. Cold season responses to the AMOC variability

When the AMOC leads Z500, the first MCA mode is 5% significant in DJF and, more so, in JFM at lags of

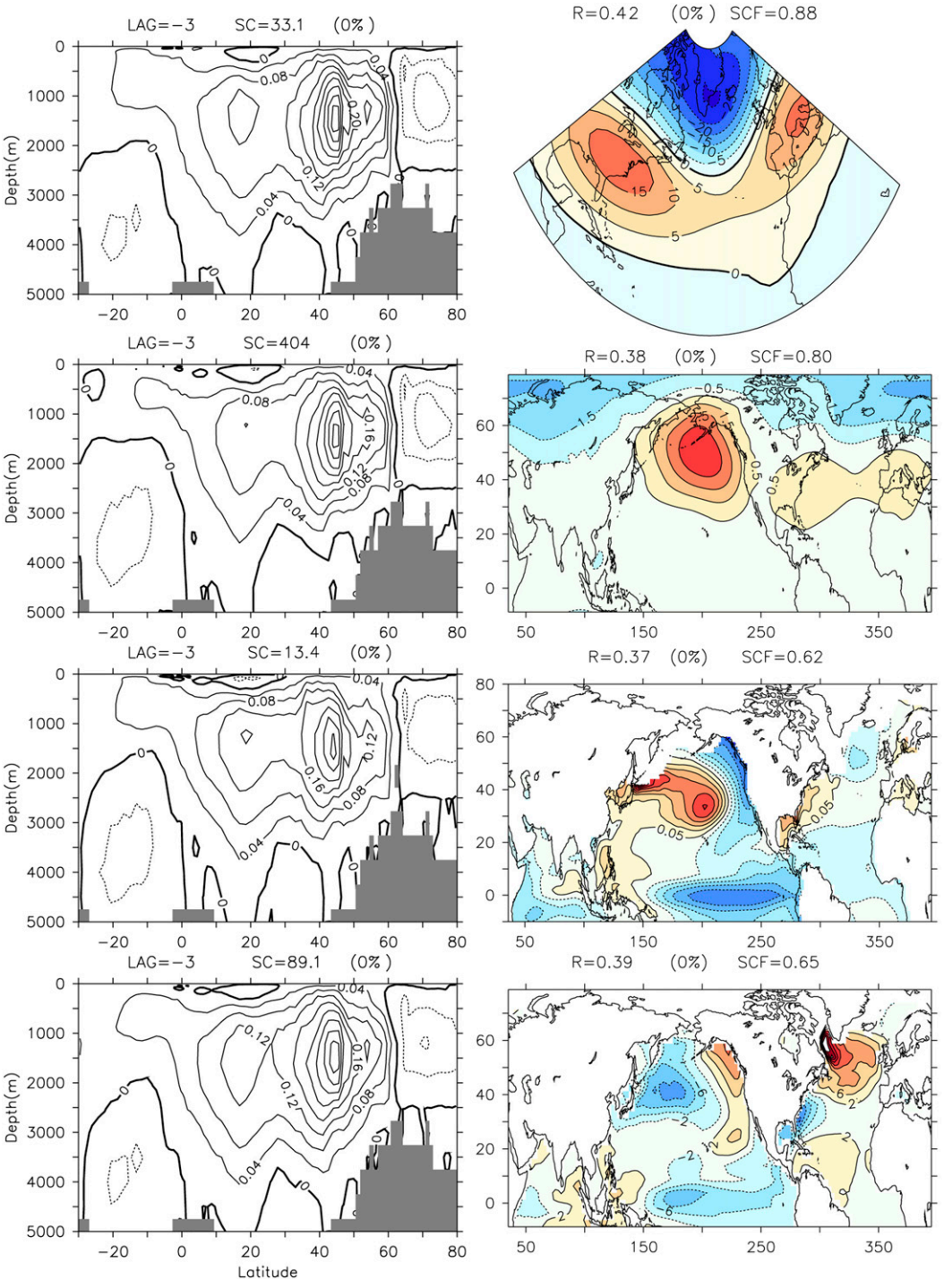

FIG. 3. First MCA mode in four separate MCA analyses when the AMOC lags by 3 yr. (top) Covariance map of (left) yearly AMOC (Sv) and (right) JFM Z500 in the Atlantic sector (m). Corresponding maps of the yearly AMOC and (second row) JFM SLP (hPa), (third row) SST (K), and (bottom) surface heat flux (W m^{-2}, positive upward), north of 10°S. Units for SC are 10^6 Sv^2 m^2, 10^2 Sv^2 hPa^2, 10^2 Sv^2 K^2, and 10^4 Sv^2 W^2 m^{-4}, respectively. Significance level of the SC and the correlation R between the MCA time series are indicated.

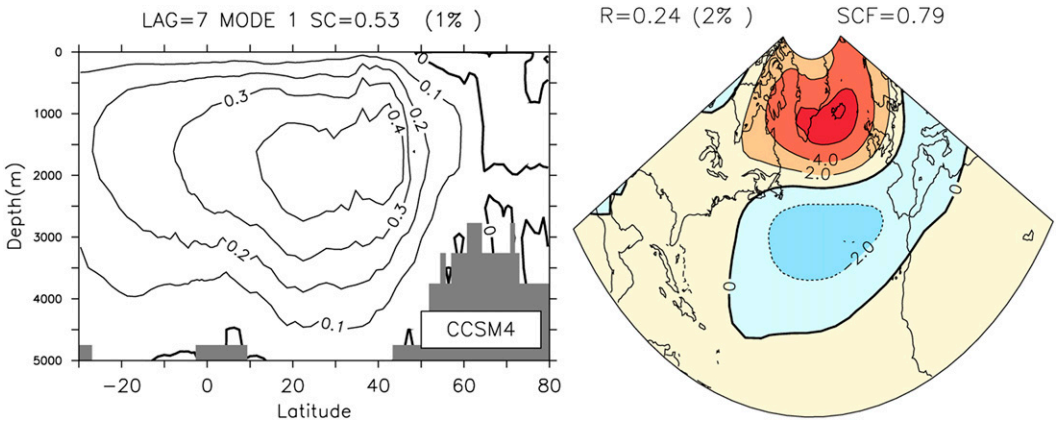

FIG. 4. Covariance map of (left) yearly AMOC (Sv) and (right) Z500 in JFM (m) for the first MCA mode when Z500 lags by 7 yr. The significance level of the SC (10^6 Sv^2 m^2) and the correlation R between the MCA time series are indicated.

7–9 yr (Fig. 2). The patterns at lag 7 are representative and shown in Fig. 4. Here, an AMOC intensification and deepening of the North Atlantic Deep Water cell that resembles the first AMOC EOF (see Fig. 2 of Danabasoglu et al. 2012b) leads by 7 yr a dipolar signal broadly resembling a negative phase of the NAO, albeit shifted slightly southward. The mode is well separated and the atmospheric response is equivalent barotropic, but the amplitude of the signal is small since, for a typical AMOC fluctuation of 0.4 Sv, the Z500 response only reaches 7 m near Iceland and 3 m off the Azores. This represents about 20% (40%) of the corresponding typical NAO amplitude near Iceland (Azores). Since the AMOC variability is largely driven by the NAO, albeit indirectly, the response should act as a weak delayed negative feedback. Note that there are only small concomitant SST anomalies in the other ocean basins, no significant Northern Hemisphere snow cover anomalies, and little Arctic sea ice cover anomalies. Hence, the atmospheric response in Fig. 4 can be attributed to the AMOC influence on the North Atlantic SST. The MCA mode in Fig. 4 has significant climate impacts, including a warming over northeast America and the Middle East and a cooling over northeast Europe (Fig. 5), decreased precipitation over the British Isles and Scandinavia, and increased precipitation over the Caucasus (not shown).

To understand what drives the atmospheric response and why it is only detected 6–9 yr after an AMOC intensification, the JFM SST anomalies were regressed on the AMOC MCA time series at lag 7, lagging them by 1–7 yr (Fig. 6, left) so that they show the time evolution of the AMOC SST fingerprint, with lag 7 corresponding to the winter Z500 signal in Fig. 4. A similar SST signature is obtained in fall, and similar patterns are also obtained by lag regression on the first AMOC PC from the EOF analysis (AMOC PC1), which is highly correlated (R = 0.82) with the AMOC MCA time series. In Fig. 7, the SST anomalies are again displayed, but with the concomitant barotropic streamfunction anomalies (left) or the mean barotropic streamfunction (right) to illustrate the influence of mean and anomalous advection. Note that very similar patterns are obtained in the subpolar gyre using the upper 500-m streamfunction instead of the barotropic one, as the subpolar gyre circulation is largely barotropic. The intensification of the AMOC is initially accompanied by a weak warming extending from the Antilles to the eastern North

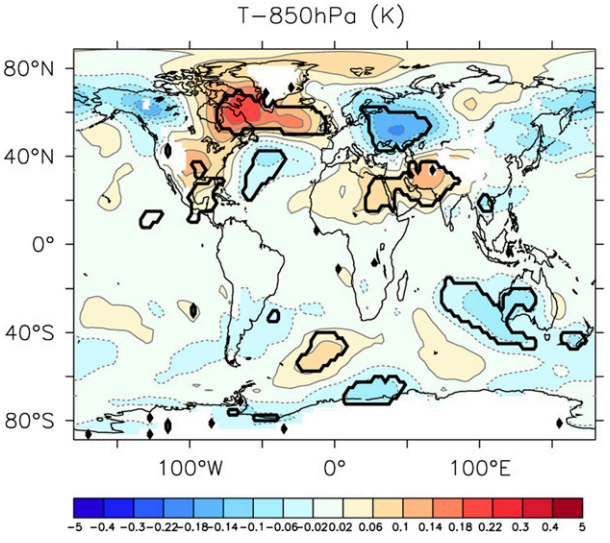

FIG. 5. Lag regression of 850-hPa temperature (K) onto the AMOC time series (from AMOC-Z500 MCA at lag 7), when AMOC leads air temperature by 7 yr. The thick black contours indicate 5% significance.

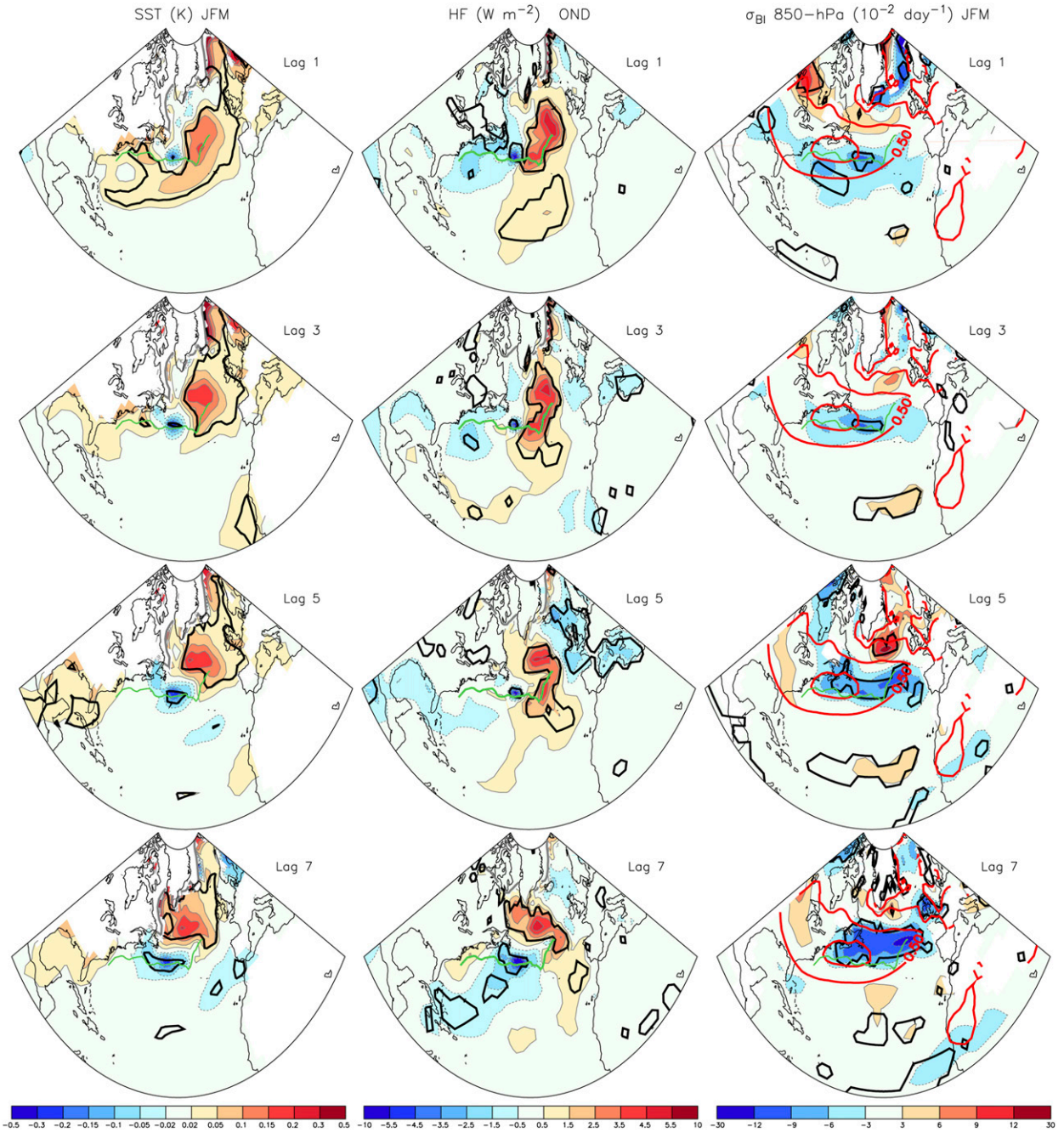

FIG. 6. Regressions of (left) JFM SST (K), (middle) OND surface heat flux (Wm^{-2}), and (right) maximum Eady growth rate (10^{-2} day^{-1}; climatology in red contours with contour at 0.5 and 0.8 day^{-1}) onto the AMOC time series from MCA at lag 7, lagging it by 1–7 yr, as indicated. The thick black contours indicate 5% significance, and the green line indicates the mean GS–NAC path.

Atlantic coast and a large warming in the midbasin along the NAC, which reflects both its northward shift and strengthening (Fig. 6 at lag 1 and Fig. 7 at lag 0). At the same time, a strengthening of the western subpolar gyre that increased the southward advection of cold subpolar water along the western boundary, together with a southward shift of the GS, cools the region southeast of Newfoundland. Note that the GS transport also increases, consistent with the AMOC intensification. As time evolves, the NAC warming intensifies and rotates cyclonically along the subpolar gyre, reflecting its advection by both the anomalous and the mean gyre circulation (lag 4 in Fig. 7), while the negative SST anomaly southeast of Newfoundland, which is very localized at

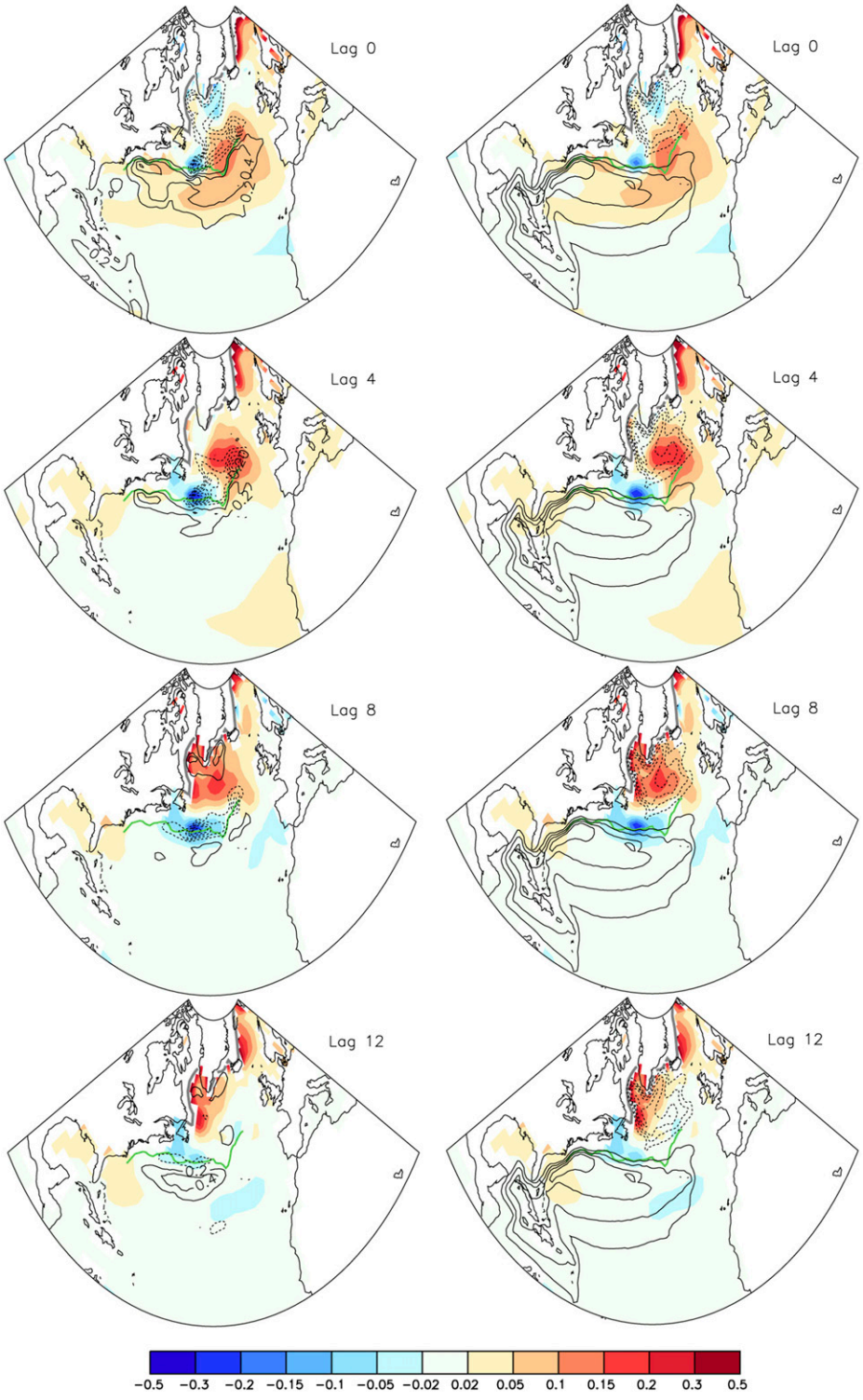

FIG. 7. Regressions of JFM SST (color; K) and (left) oceanic barotropic streamfunction (black line; dashed for cyclonic flow; contour interval: 0.2 Sv; zero-line omitted) onto the AMOC time series from MCA at lag 7, lagging it by 0–12 yr, as indicated. The green line indicates the mean GS–NAC path, and the thick gray line the sea ice edge. (right) The thin line shows the mean barotropic streamfunction (contour interval: 10 Sv; zero-line omitted).

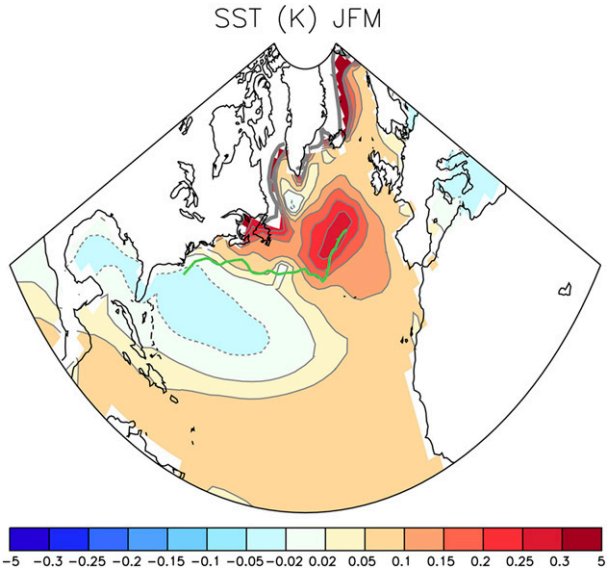

FIG. 8. Winter AMO pattern in CCSM4 as derived from a regression of JFM SST onto the yearly AMO time series, defined as the averaged 10-yr low-passed SST in the North Atlantic (75°W–7.5°E, 0°–60°N). The green line indicates the mean GS–NAC path.

lag 1, expands eastward and intensifies. By lag 6 (not shown), the advection along the mean streamfunction prevails, and a robust SST anomaly dipole in the meridional/southwest–northeast direction is established. A typical AMOC intensification has warmed the subpolar gyre by about 0.2 K, while the GS–western NAC region has cooled by 0.2 K (see lag 7 and 8). The SST pattern broadly resembles the model AMO, but it is shifted ~15° latitude to the north, and the AMO lacks the GS cooling (Fig. 8; see also in Danabasoglu et al. 2012b). As illustrated for lag 12 (Fig. 7), it is found that at lag larger than 9, the dipole weakens, as the subpolar warming is increasingly confined to the western part of the basin, mostly by mean advection, and the GS cooling decreases, consistent with the loss of statistical significance in the MCA.

The evolution of surface heat fluxes and SST anomalies are similar and indicate that the heat fluxes damp the SST anomalies. This is seen until about lag 5, although the negative turbulent heat flux feedback is too weak in CCSM4 (Bates et al. 2012). However, it is not seen at larger lag in the JFM surface heat fluxes, as it is masked by the heat flux anomalies associated with the atmospheric JFM response, which is illustrated in Fig. 9 (top). The negative heat flux feedback is recovered, albeit somewhat noisily, when the heat flux signature of the large-scale atmospheric response (middle) is subtracted (bottom). The heat flux induced by the atmospheric response is based on the regression of the surface heat flux onto the Z500 MCA time series at lag 7, times

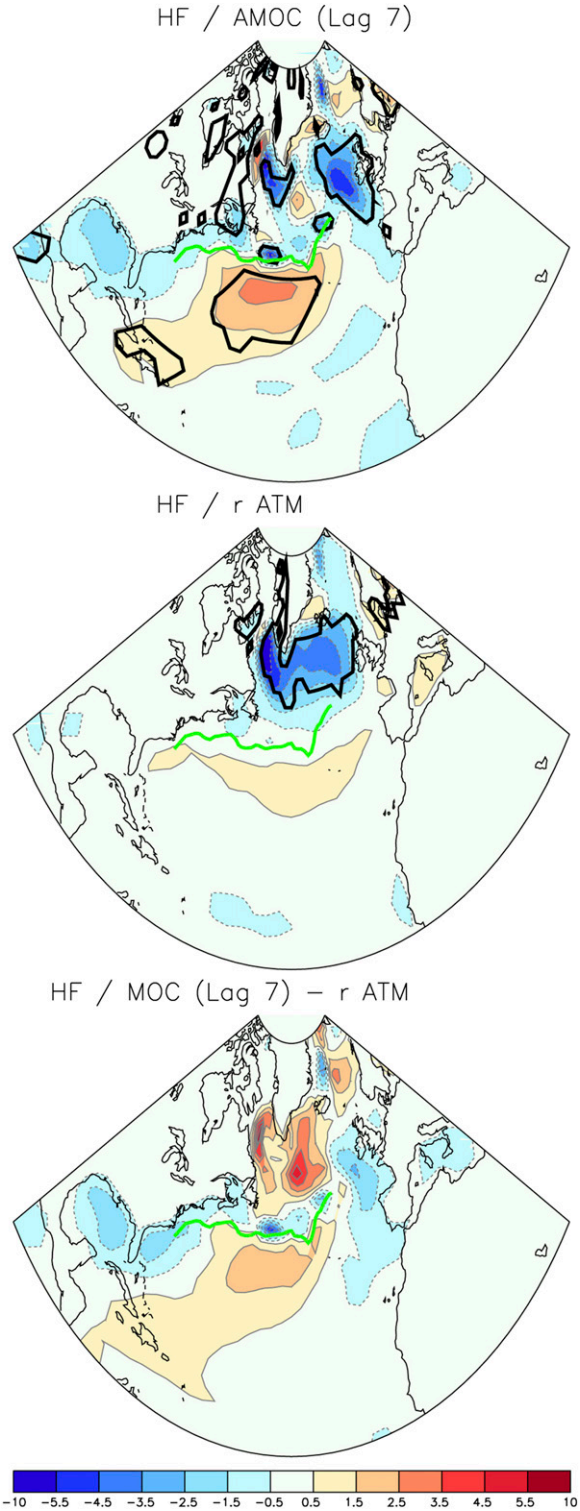

FIG. 9. Regression of upward surface heat flux (Wm^{-2}) in JFM onto (top) the AMOC MCA time series at lag 7, when AMOC leads the heat flux by 7 yr, and (middle) the Z500 MCA time series multiplied by its correlation R with the AMOC one. (bottom) Difference between (top) and (middle). The thick black contours indicate 5% significance, and the green line the mean GS–NAC path.

the correlation of the latter with the AMOC time series, as in Gastineau and Frankignoul (2012). The negative heat flux feedback appears more clearly in October–December (OND), when no large-scale atmospheric response is detected and the SST fingerprint is similar, albeit slightly weaker; hence, its time evolution is shown for OND in Fig. 6 (middle). The anomalous OND surface heat release closely reflects the SST changes and similarly evolves cyclonically along the subpolar gyre while an anomalous oceanic heat gain develops in the GS region, leading to an anomalous dipolar heating and cooling of the atmosphere. The anomalous heating affects baroclinicity in the lower troposphere and the growth of the synoptic transient eddies, which is measured by the maximum Eady growth rate $0.31f|\partial\mathbf{U}/\partial z|N^{-1}$, with f the Coriolis parameter, $\mathbf{U}$ the horizontal wind, z the height, and N the Brunt–Väisälä frequency (Hoskins and Valdes 1990). The anomalous maximum Eady growth rate at 850 hPa (Fig. 6, right), which is small at lag 1, shows a negative anomaly moving westward into the region of maximum Eady growth rate and a decrease of the lower-tropospheric baroclinicity (see lag 5). By lag 7, the region of maximum baroclinicity has also moved southward, because of the decreased meridional SST gradient. As a result, there is a slight southward shift of the transient eddy activity (not shown). As shown by Rivière (2009), cyclonic wave breaking of synoptic eddies is more frequent when the low-level baroclinicity is more southward. This leads to a convergence of momentum flux south of the upper-tropospheric jet and pushes it southward, which renders cyclonic wave breaking more probable so that the jet is more zonally oriented and maintained more southward by a positive eddy feedback, which explains a negative NAO phase.

In CCSM4, the wintertime NAO-like response to the AMOC is similar to that seen in the 6 climate models discussed by Gastineau and Frankignoul (2012), but the amplitude is about twice as small, reflecting the too small heat flux feedback. Because of the smaller signal-to-noise ratio, the AMOC impact during winter could not be detected at the seasonal scale from SST alone. Indeed, no robust winter mode could be found in a lag MCA with North Atlantic SST leading Z500 during winter. Correspondingly, no atmospheric response to the seasonal SST anomalies corresponding to the model AMO (pattern defined by the regression on the 10-yr low-passed North Atlantic SST averaged over 0°–60°N, 75°W–7.5°E) could be found in winter using lagged regression, even after ¼–½–¼ smoothing. Note that the JFM AMO pattern (Fig. 8) is broadly realistic, although its amplitude is smaller than in the observations. It shows some similarity with the AMOC fingerprint at lag 7 (cf. with Fig. 6), although the subpolar warming takes place farther southward, and the GS region is anomalously warm instead of cold. Presumably, the differences occur because the AMO pattern emphasizes low-frequency variations and mixes SST preceding and lagging the AMOC. In addition, direct atmospheric forcing also influences the AMO. In any case, the weakening of the meridional SST gradient is about twice as small in the AMO pattern than in the AMOC footprint, and it is displaced substantially southward. This, coupled with the northerly bias in the mean tropospheric jet in the North Atlantic in CCSM4 (Davini and Cagnazzo 2014), may explain why no atmospheric response to the AMO could be found in the cold season, either by regression or MCA.

6. Links to the variability of the North Atlantic Ocean circulation

The impact of the AMOC variability on winter climate is closely linked to the meridional shifts of the GS and the NAC and to the strengthening of the subpolar gyre. However, their timing needs to be explained. The variability of the GS–NAC position, which is maximum near 36°–40°W (blue squares in Fig. 1), is dominated by interannual frequencies, and it shows only limited zonal coherence. There is more zonal coherence at low frequency, however, and there are persistent links with the AMOC. Therefore, the GS–NAC variability and associated SST anomalies in relation with the AMOC changes are first discussed before analyzing other aspects of the atmosphere–ocean interaction associated with the GS–NAC variability.

As shown in the lag correlation between the GS–NAC position at each longitude and AMOC PC1 for ¼–½–¼-smoothed data (Fig. 10), the GS–western NAC (42°–52°W) shifts southward after the maximum AMOC intensification, while the NAC near the Mid-Atlantic Ridge (28°–33°W) shifts northward immediately following the AMOC intensification, which is consistent with the zonal dipole pattern of SST anomalies along the GS–NAC in Fig. 6 at lag 1. The strongest and most persistent correlation occurs when the AMOC leads the GS–NAC between 42° and 47°W by 3–9 yr, but a significant southward shift of the GS already precedes the AMOC by several years. On the other hand, the northward shift near the Mid-Atlantic Ridge lasts only a few years, and after 6 yr, the NAC starts shifting south, which is also consistent with the time evolution of the positive SST anomalies shown in Figs. 6 and 7, suggesting the downstream propagation of the anomalies.

As discussed by Danabasoglu et al. (2012b), a stronger subpolar gyre precedes a stronger AMOC. It can be shown by regression on AMOC PC1 that an

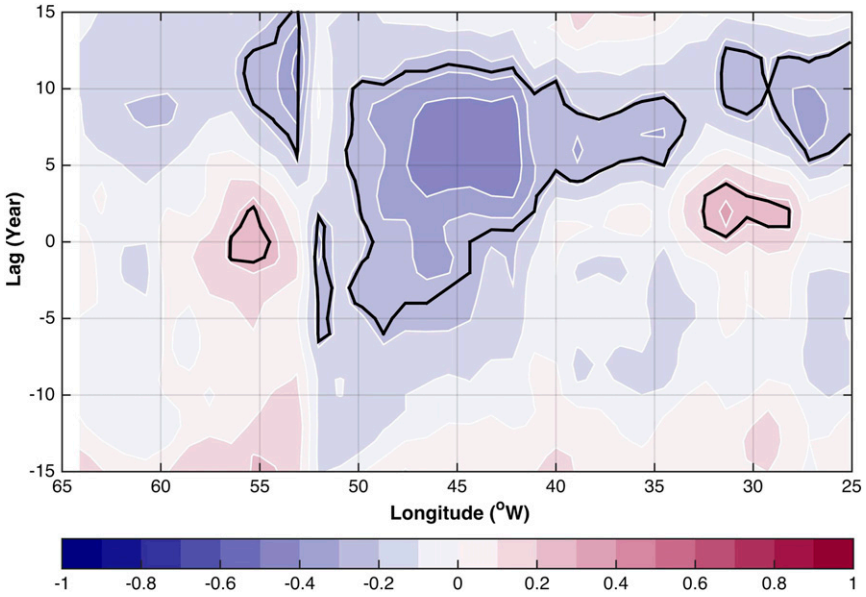

FIG. 10. Lag correlation between the GS–NAC meridional position at each longitude and AMOC PC1 after binomial smoothing. AMOC leads at positive lags. The black contours indicate 5% significance.

intensification of the western subpolar gyre and its southward, nearly barotropic deep western boundary current precedes the AMOC intensification by several years. This brings cold subpolar water toward the Tail of the Grand Banks, as seen at lag 0 in Fig. 7, and shifts the GS southward. Cold water advection prevails at first over the southward shift of the GS in cooling the SST southeast of the Tail of the Grand Banks, while the GS shift dominates the cooling after the AMOC maximum. The SST anomalies are collocated with the continental slope (Fig. 11), which suggests that the southward GS shift results from the interaction between the deep flow and topography. Zhang and Vallis (2007) suggested that the southward deep western boundary current near the Tail of the Grand Banks would move downslope because of bottom Ekman transport and bottom torque. The resulting bottom downwelling would lead to a positive vorticity through bottom vortex stretching, which contributes to the formation of the northern recirculation gyre and shifts the GS southward. Although there is no northern recirculation gyre in CCSM4, this mechanism should still be valid, but it takes place farther east, where the GS separates from the coast. Consistent with this mechanism, the AMOC is significantly correlated near the Tail of the Grand Banks (44°–45°N, 42°–47°W) with both the curl of the deep velocity (i.e., anomalous cyclonic circulation for an AMOC increase) and the southward shift of the GS (Fig. 12). The highest correlation between the AMOC and the curl of the deep velocity is $R = 0.48$ (0.72) when AMOC PC1 leads by 3 yr (but similar for lag = −1–4 yr) without any low-pass filtering (with 10-yr low-pass filtering), and the correlation between the positive curl of the deep velocity and the southward GS shift peaks when the GS lags by 1 yr,

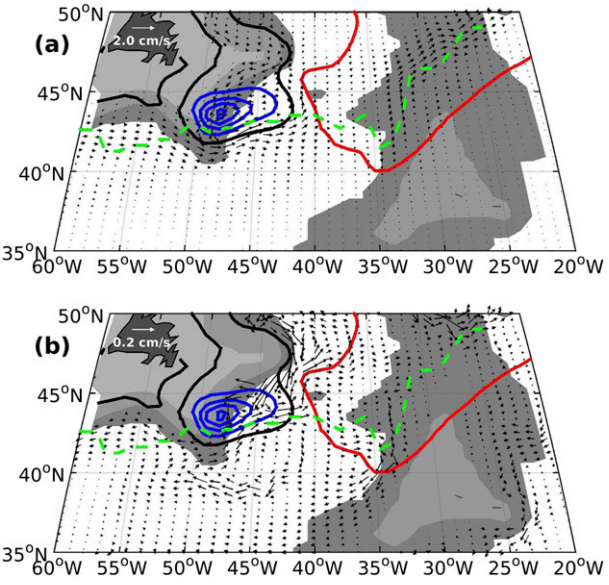

FIG. 11. Regressions of SST (0.1-K contour interval) and (a) 0–500-m and (b) 2000–3000-m velocity (vectors) on AMOC PC1, when AMOC PC1 leads by 1 yr. A binomial smoothing was applied before the regression. Contours indicate positive (red), negative (blue), and zero (black) SST anomalies. The green dashed line is the mean GS–NAC position. Gray shading from light to dark indicates 500-, 2500-, and 4000-m isobaths.

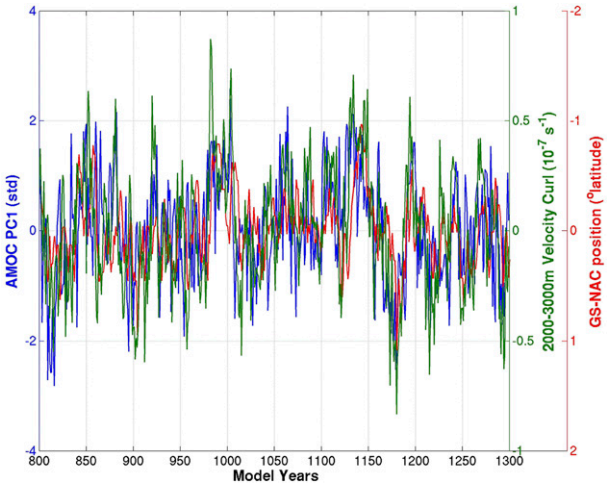

FIG. 12. Time series of yearly AMOC PC-1 (blue), curl of deep velocity (green; averaged over 2000–3000 m and 44°–45°N, 42°–47°W), and GS–NAC latitude (red; averaged over 42°–47°W). Note that the *y* axis for the GS–NAC latitude is reversed.

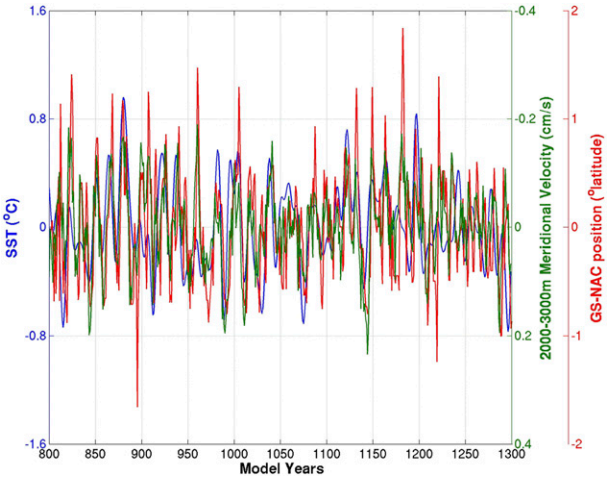

FIG. 13. Time series of annual mean SST (blue; 44°–48°N, 27°–33°W), deep meridional velocity (green; averaged over 2000–3000 m and 44°–48°N, 27°–33°W), and NAC latitude near the Mid-Atlantic Ridge (red; averaged over 27°–33°W). Note that the *y* axis for the deep meridional velocity is reversed.

reaching 0.65 without any low-pass filtering. The results are similar if the upper-ocean velocity is considered because of the barotropic nature of the current there (Fig. 11a). Note that the cyclonic vorticity of the upper water column is shifted upslope as mass is removed, coinciding better with the cold SST anomaly. See Yeager (2015) for an in-depth discussion of the role of bottom pressure torque in the variability of the AMOC.

As discussed earlier, the equatorward deep flow exhibits interior pathways and crosses the NAC near the western flank of the Mid-Atlantic Ridge (Fig. 1b). Regression on the AMOC PC1 shows increased southward deep velocity along the western flank of the Mid-Atlantic Ridge (~33°W) as well as a warm SST anomaly collocated with the NAC mean position (Fig. 11). Kwon and Frankignoul (2014) suggested that crossover between deep equatorward flow and NAC near the western flank of the Mid-Atlantic Ridge would generate in CCSM3 a northward shift of NAC when the southward deep flow was stronger, which is opposite to the situation on the western boundary because of the much gentler and opposite-signed bottom slope, resulting in a vortex squeezing. Similarly, near the Mid-Atlantic Ridge (averaged over 44°–48°N, 27°–33°W), a stronger southward deep velocity (at 2000–3000 m) in CCSM4 is significantly correlated with a northward shift of the NAC position (Fig. 13), with maximum correlation $R = -0.78$ occurring at no lag (−0.88 with 10-yr low-pass filter). In the same region, a northward NAC shift is significantly correlated with warmer SST (Fig. 13), with $R = 0.45$ (0.57 with 10-yr low-pass filter). The SST anomaly is weaker than in the GS region, where the mean meridional SST gradient is larger, and the anomalous currents are stronger. Note that, as discussed earlier, the strengthening of the NAC also contributes to the warming.

Using the averaged GS–NAC latitude in 42°–47°W as an index (GS–NAC index) of its meridional displacements shows that a southward shift of the GS–NAC is indeed preceded by an EOF1-like basinwide AMOC intensification (Fig. 14), together with a strengthening of the subtropical and the subpolar gyres (not shown), with maximum negative correlation when the AMOC leads by 6 yr. At shorter lag, the AMOC intensification decreases while a weakening of the northern subpolar gyre appears, and both decay when the AMOC lags by a few years. There is also a strong intergyre gyre (a circulation anomaly that crosses from one gyre to the other, Marshall et al. 2001) covarying with the GS–NAC index (not shown), which reflects the gyre response to the NAO wind stress curl forcing. In fact, a negative NAO precedes a southward shift of the GS–NAC, as shown in Fig. 15 by the MCA between the GS–NAC position and Z500 when Z500 leads by 1 yr (no binomial smoothing was applied to emphasize the fast GS–NAC response), consistent with the observations (e.g., Frankignoul et al. 2001). Therefore, the NAO drives GS–NAC shifts not only through the AMOC changes, but also more directly through the changes in the wind-driven circulation. At longer lag, the sign reverses, and a positive NAO leads a southward shift of the GS–NAC, presumably reflecting its indirect impact via the AMOC intensification.

In phase with or just following the southward GS–NAC shift in 42°–47°W, there is, as expected, a strong

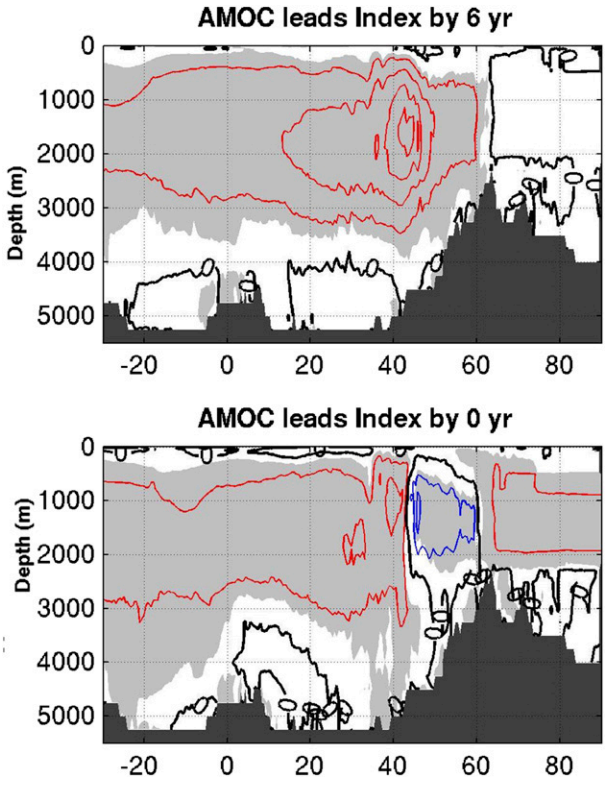

FIG. 14. Regression of the yearly AMOC [contour interval: 0.1 Sv; positive (red); negative(blue)] onto the $-1 \times$ GS–NAC index (averaged latitude in 42°–47°W) when the AMOC (top) leads by 6 yr or (bottom) varies in phase. Note that the regressions correspond to a southward shift of the GS. Shading indicates 5% significance.

cooling near (42°–45°N, 40°–50°W). However, there is also a broader warming in the subpolar gyre (Fig. 16 left, shown for comparison with Fig. 6 after ENSO removal and ¼–½–¼ filtering) so that the SST anomalies associated with a southward GS–NAC shift resemble the meridional SST dipole following the AMOC by about 7 yr (Fig. 6, bottom), albeit with a slightly larger amplitude and a stronger and broader GS–NAC cooling. The SST is (weakly) damped by the surface turbulent heat flux at a rate of about 10 $\mathrm{W\,m^{-2}\,K^{-1}}$ that is 2–3 times weaker than in the observations (Frankignoul and Kestenare 2002; Park et al. 2005). Yet no significant Z500 response to the GS shifts could be detected by lag MCA or lag regression on the GS–NAC index.

The lack of response to the GS–NAC shift seems primarily because of the interference with the atmospheric response to concomitant North Pacific SST anomalies. Indeed, because the NAO in CCSM4 resembles an annular mode (Davini and Cagnazzo 2014), a negative NAO is associated with a weakening of the Aleutian low (Fig. 15, right). Hence, a negative NAO also drives an SST anomaly in the North Pacific that resembles its first mode of variability [associated with the Pacific decadal oscillation (PDO)], while no significant North Pacific SST anomaly is associated with the AMOC at lag 7 (consistent with Fig. 5). To determine whether the North Pacific SST in turn influences the atmosphere, we performed a lag MCA between 3-month-averaged North Pacific SST and JFM Z500 after applying a binomial smoothing (¼–½–¼) to both the Z500 and SST time series. As shown in Fig. 17 (top) and discussed by Deser et al. (2012), the variability of the Aleutian low drives a PDO-like SST anomaly in CCSM4, which shows some resemblance with the pattern in Fig. 16. More importantly, an SST anomaly that more closely resembles the one that covaries with a southward GS shift (Fig. 16) influences the winter atmospheric circulation not only in the North Pacific (Deser et al. 2012), but also in the North Atlantic sector, where it resembles a positive NAO (Fig. 17, bottom). Hence, this positive Arctic Oscillation–like response opposes the negative NAO-like response to the meridional SST dipole associated with the GS–NAC southward shift. On the other hand, the 6–9-yr separation between the AMOC forcing and the NAO-like response effectively disconnect the PDO interference. The atmospheric response to the NAO-driven sea ice concentration seesaw between the Labrador and the Greenland–Barents Seas (to be discussed elsewhere) may also introduce additional noise.

7. Summary and discussion

Danabasoglu et al. (2012b) showed that the AMOC variability is primarily driven in CCSM4 by salinity-dominated density anomalies at the Labrador Sea deep-water convection site and subpolar gyre circulation changes, and they speculated that the latter were set by the NAO, which thus had mostly an indirect influence. Using MCA, we have shown that the NAO indeed contributes to driving the AMOC variability and that the AMOC is also influenced by ENSO, presumably because the ENSO teleconnection is too strong in the model. We have also shown that an equivalent barotropic signal in winter broadly resembling a negative phase of the NAO follows an AMOC intensification by about 7 yr. The delay is caused by the cyclonic propagation along the NAC and the subpolar gyre of a growing SST warming, which follows the AMOC intensification, together with an increasing SST cooling southeast of the Tail of the Grand Banks. This results in a meridional SST dipole after 6 or 7 yr. The AMOC SST fingerprint is consistent with the AMOC fingerprints suggested by Zhang (2008).

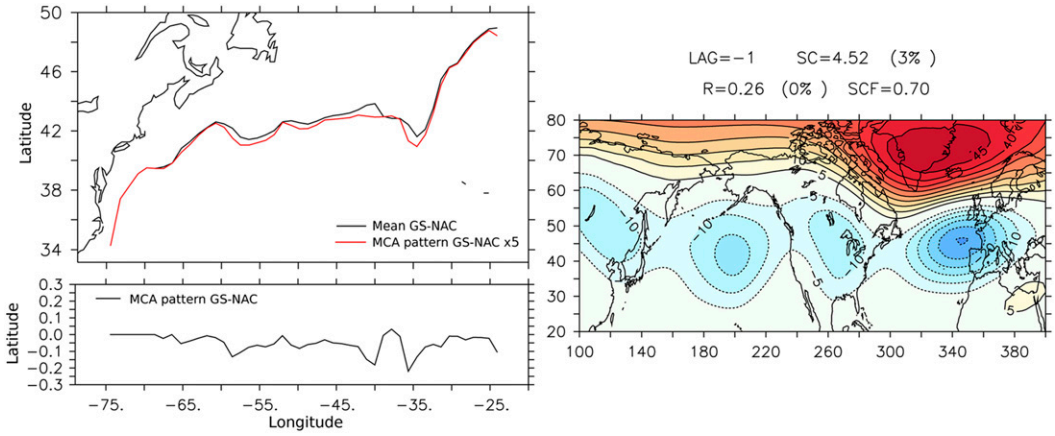

FIG. 15. (left) Covariance map of the GS–NAC position (° lat) and (right) Z500 in JFM in the North Atlantic sector (m) for the first MCA mode when Z500 leads by 1 yr (no binomial smoothing has been applied). Significance level of the SC and the correlation R between the MCA time series is indicated. The Z500 signal over the North Pacific was obtained by regression on the Z500 MCA time series. (bottom left) The anomalous meridional displacement of the GS position; (top left) the climatological mean position of the GS–NAC (black) and the mean plus anomalies, with the anomalies in latitude multiplied by 5 for clarity (red).

We have argued that the AMOC SST fingerprint reflects both SST advection by the subpolar gyre and opposite bottom torque near the Tail of the Grand Banks and the western flank of the Mid-Atlantic Ridge, where the crossover of the deep branches of the AMOC and the GS–NAC occur. When the AMOC intensifies, the southward deep western boundary current strengthens, and cold SST anomalies appear just north of the GS along the continental slope. The latter reflect both the intensification of the western subpolar gyre that increases the southward advection of cold water and a southward shift of the GS. The latter is caused by the vortex stretching and cyclonic vorticity induced by bottom Ekman transport and bottom torque as the deep current moves downslope, as shown by Zhang and Vallis (2007), which is also found in the upper ocean, albeit shifted upslope, because the current is barotropic. Both processes lead the AMOC by several years, consistent

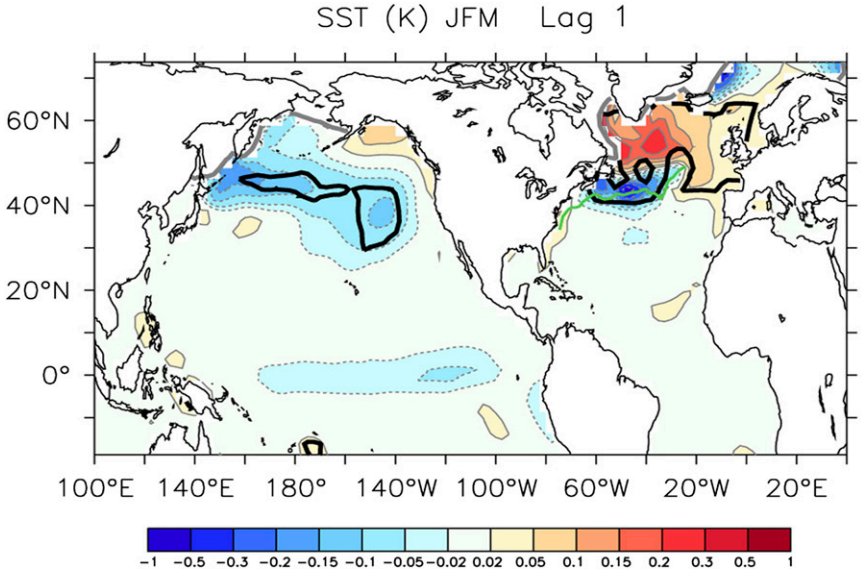

FIG. 16. Regression of SST (K) in JFM onto the −1 × GS–NAC index after ENSO removal and low-pass filtering, when the −1 × GS–NAC index leads by 1 yr. The thick black contours indicate 5% significance, and the green line the mean GS–NAC path. Note that the regression corresponds to a southward shift of the GS.

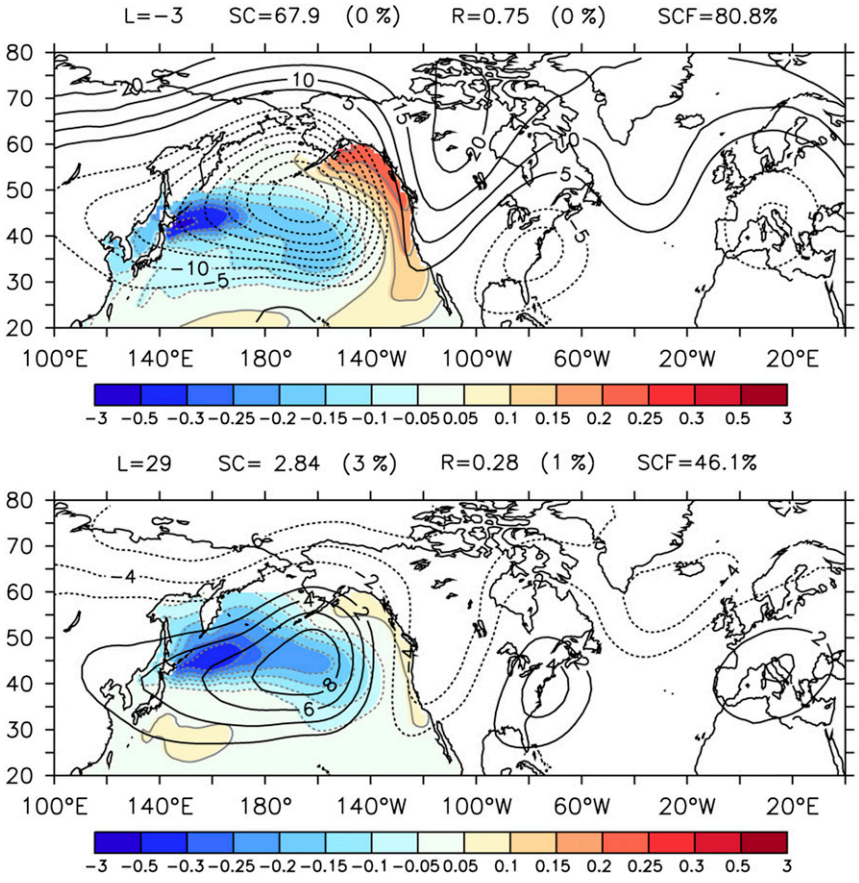

FIG. 17. Covariance map of low-pass filtered North Pacific SST (K) and JFM Northern Hemisphere Z500 (m) when (top) Z500 leads by 3 months and (bottom) SST leads by 29 months. Significance levels of SC and *R* are indicated.

with Danabasoglu et al. (2012b), who showed that a stronger subpolar gyre precedes a stronger AMOC, with southward advection prevailing at first over the southward shift of the GS shift in cooling the SST, while the GS shift dominates the cooling after the AMOC maximum. The equatorward deep flow also exhibits interior pathways and crosses the NAC near the western flank of the Mid-Atlantic Ridge. As the southward deep flow intensifies, it causes a northward shift of the NAC and a surface warming, which is opposite to the situation on the western boundary, because of the much gentler and opposite-signed bottom slope resulting in a vortex squeezing, as suggested by Kwon and Frankignoul (2014). The intensification of the NAC and the subpolar gyre also contribute to driving and enhancing the SST warming.

As the surface heat flux damps the resulting SST anomalies, there are anomalous air–sea heat exchanges. When forming a meridional dipole, they reduce and shift slightly southward the baroclinicity of the lower atmosphere in the region of maximum growth of the transient eddies, as shown by the anomalous Eady growth rate. This results in a slight southward shift of the North Atlantic storm track and negative NAO-like response. A similar NAO-like response to an AMOC intensification was found in the six climate models discussed in Gastineau and Frankignoul (2012). However, the atmospheric response in CCSM4 has a smaller amplitude, typically reaching only 5 m at 500 hPa and 0.55 hPa at sea level, which is twice as small as that found in other climate models (Gastineau and Frankignoul 2012). This reflects both the small amplitude of the AMOC fluctuations (Danabasoglu et al. 2012b) and the too weak heat flux feedback in CCSM4 (Bates et al. 2012). As a result, the signal-to-noise ratio is small, which may explain why the AMOC influence on the winter atmosphere could not be detected at the seasonal scale from SST alone, unlike in IPSL-CM5 (Gastineau et al. 2013).

Similar mechanisms were at play in CCSM3, the previous version of the NCAR climate model. Indeed, Kwon and Frankignoul (2014) have shown that the SST

fingerprint of the AMOC variability was similarly controlled by the crossover between the GS–NAC and the two branches of deep equatorward flow. However, in the red-noise AMOC regime found in the latter part of the CCSM3 control simulation, the SST anomaly caused by an AMOC intensification reflected a northward shift of the entire GS–NAC system and thus a northward shift of the region of maximum heat release to the atmosphere and of maximum synoptic growth. This leads to a positive NAO-like response, opposite to the negative NAO-like response detected in CCSM4. The response was twice as large as in CCSM4 because of the larger AMOC SST footprint, but the AMO pattern was not realistic. In any case, the physics of the AMOC influence appears to be similar in all the models: the response occurs when the SST footprint of the AMOC alters the meridional SST gradient and modulates the low-level baroclinicity. In addition our result is also consistent with the northward shift and elongation of the North Atlantic storm track associated with the weakening of AMOC in future climate change simulations (Woollings et al. 2012).

On the other hand, in CCSM4 we could not detect a significant cold season atmospheric response to the AMO, which is broadly realistic but weaker than observed and displaced southward, presumably because of a small signal-to-noise ratio and mismatch with the jet location. The model AMO shows some similarity with the AMOC fingerprint at about 7-yr lag, when an atmospheric response is detected, but the subpolar warming is found farther southward, and the GS region is anomalously warm instead of cold. Hence, the weakening of the meridional SST gradient is about twice as small in the AMO pattern as in the AMOC footprint, and it is displaced substantially southward. Nonetheless, since the AMO lags the AMOC at low frequency by about 2 yr (Danabasoglu et al. 2012b), the negative NAO-like response to the AMOC is consistent with the negative NAO-like response to the AMO seen in the observations and atmospheric response studies (Peings and Magnusdottir 2014; Omrani et al. 2014; Gastineau and Frankignoul 2015).

Whether the estimated winter response found in different climate models or in the observations scales with the change in meridional temperature gradient can only be coarsely estimated. In IPSL-CM5-LR, where a negative NAO-like winter response to an AMOC amplification was found after a delay of about 9 yr (Gastineau and Frankignoul 2012), the meridional SST gradient anomaly was substantially larger than in CCSM4 [1.1 K $(10°)^{-1}$ vs 0.4 K $(10°)^{-1}$] and similarly located, yet the response amplitude was only twice as large (1 vs 0.55 hPa), despite a stronger heat flux damping. This suggests that CAM4, the atmospheric component of CCSM4, is more sensitive to boundary forcing than the atmospheric components of IPSL-CM5 or CCSM3. In the observational analysis of Gastineau and Frankignoul (2015), the meridional temperature gradient associated with the AMO is about 0.5 K $(10°)^{-1}$ (when corrected for SST decay), and the negative NAO-like response reaches 25 m at 500 hPa. This compares rather well with the estimated response to the AMOC in CCSM4 (6 m at 500 hPa), if one takes into account the underestimation by a factor of 3 of the heat flux feedback. As the meridional temperature gradient associated with the AMO in CCSM4 is only about 0.1 K $(10°)^{-1}$, the signal-to-noise ratio was too small, and no winter response to the AMO could be detected. However, one important fact that is not taken into consideration in these rough comparisons is the differences in the degree of proximity between the meridional SST gradient anomalies and the mean atmospheric jet and the storm-track path among different models and observations. Finally, we could not detect an atmospheric response to the meridional shifts of the GS–NAC in CCSM4, even though their dipolar SST signature was broadly similar to that driven by the AMOC. This seems primarily caused by an NAO-like response of the opposite sign to the North Pacific SST anomalies that covary with the GS–NAC shifts, as both respond to the too-zonally symmetric NAO in CCSM4.

Acknowledgments. Support from the NOAA Climate Program Office (NA10OAR4310202 and NA13OAR4310139), NSF EaSM2 (OCE 1242989) and the European Community 7th framework programme (FP7 2007-2013) under Grant Agreement 308299 (NACLIM) is gratefully acknowledged. The analysis benefited from the IPSL Prodiguer-Ciclad facility, which is supported by CNRS, UPMC, Labex L-IPSL funded by the ANR (Grant ANR-10-LABX-0018) and by the European FP7 IS-ENES2 project (Grant 312979). We thank the reviewers for their insightful comments and helpful suggestions.

REFERENCES

Alexander, M. A., and C. Deser, 1995: A mechanism for the recurrence of wintertime midlatitude SST anomalies. *J. Phys. Oceanogr.*, **25**, 122–137, doi:10.1175/1520-0485(1995)025<0122:AMFTRO>2.0.CO;2.

Bates, S. C., B. Fox-Kemper, S. R. Jayne, W. G. Large, S. Stevenson, and S. G. Yeager, 2012: Mean biases, variability, and trends in air–sea fluxes and sea surface temperature in the CCSM4. *J. Climate*, **25**, 7781–7801, doi:10.1175/JCLI-D-11-00442.1.

Bower, A. S., M. S. Lozier, S. F. Gary, and C. W. Böning, 2009: Interior pathways of the North Atlantic meridional overturning circulation. *Nature*, **459**, 243–248, doi:10.1038/nature07979.

Bretherton, C. S., C. Smith, and J. M. Wallace, 1992: An intercomparison of methods for finding coupled patterns in climate data. *J. Climate*, **5**, 541–560, doi:10.1175/1520-0442(1992)005<0541:AIOMFF>2.0.CO;2.

Czaja, A., and C. Frankignoul, 2002: Observed impact of Atlantic SST anomalies on the North Atlantic Oscillation. *J. Climate*, **15**, 606–623, doi:10.1175/1520-0442(2002)015<0606:OIOASA>2.0.CO;2.

Danabasoglu, G., S. Bates, B. P. Briegleb, S. R. Jayne, M. Jochum, W. G. Large, S. Peacock, and S. G. Yeager, 2012a: The CCSM4 ocean component. *J. Climate*, **25**, 1361–1389, doi:10.1175/JCLI-D-11-00091.1.

——, S. G. Yeager, Y.-O. Kwon, J. J. Tribbia, A. S. Phillips, and J. W. Hurrell, 2012b: Variability of the Atlantic meridional overturning circulation in CCSM4. *J. Climate*, **25**, 5153–5172, doi:10.1175/JCLI-D-11-00463.1.

Davini, P., and C. Cagnazzo, 2014: On the misinterpretation of the North Atlantic Oscillation in CMIP5 models. *Climate Dyn.*, **43**, 1497–1511, doi:10.1007/s00382-013-1970-y.

de Coëtlogon, G., and C. Frankignoul, 2003: The persistence of winter sea surface temperature in the North Atlantic. *J. Climate*, **16**, 1364–1377, doi:10.1175/1520-0442-16.9.1364.

Deser, C., and Coauthors, 2012: ENSO and Pacific decadal variability in Community Climate System Model version 4. *J. Climate*, **25**, 2622–2651, doi:10.1175/JCLI-D-11-00301.1.

Deshayes, J., and C. Frankignoul, 2005: Spectral characteristics of the response of the meridional overturning circulation to deep-water formation. *J. Phys. Oceanogr.*, **35**, 1813–1825, doi:10.1175/JPO2793.1.

Enfield, D. B., A. M. Mestas-Nuñez, and P. J. Trimble, 2001: The Atlantic Multidecadal Oscillation and its relation to rainfall and river flows in the continental U.S. *Geophys. Res. Lett.*, **28**, 2077–2080, doi:10.1029/2000GL012745.

Frankignoul, C., and E. Kestenare, 2002: The surface heat flux feedback. Part I: Estimates from the observations in the Atlantic and the North Pacific. *Climate Dyn.*, **19**, 663–647, doi:10.1007/s00382-002-0252-x.

——, G. de Coëtlogon, T. M. Joyce, and S. Dong, 2001: Gulf Stream variability and ocean–atmosphere interactions. *J. Phys. Oceanogr.*, **31**, 3516–3529, doi:10.1175/1520-0485(2002)031<3516:GSVAOA>2.0.CO;2.

——, N. Sennéchael, Y.-O. Kwon, and M. A. Alexander, 2011: Influence of the meridional shifts of the Kuroshio and the Oyashio Extensions on the atmospheric circulation. *J. Climate*, **24**, 762–777, doi:10.1175/2010JCLI3731.1.

——, G. Gastineau, and Y. O. Kwon, 2013: The influence of the AMOC variability on the atmosphere in CCSM3. *J. Climate*, **26**, 9774–9790, doi:10.1175/JCLI-D-12-00862.1.

Gastineau, G., and C. Frankignoul, 2012: Cold-season atmospheric response to the natural variability of the Atlantic meridional overturning circulation. *Climate Dyn.*, **39**, 37–57, doi:10.1007/s00382-011-1109-y.

——, and ——, 2015: Influence of the North Atlantic SST variability on the atmospheric circulation during the twentieth century. *J. Climate*, **28**, 1396–1416, doi:10.1175/JCLI-D-14-00424.1.

——, F. D'Andrea, and C. Frankignoul, 2013: Atmospheric response to the North Atlantic Ocean variability on seasonal to decadal time scales. *Climate Dyn.*, **40**, 2311–2330, doi:10.1007/s00382-012-1333-0.

Gent, P. R., and Coauthors, 2011: The Community Climate System Model version 4. *J. Climate*, **24**, 4973–4991, doi:10.1175/2011JCLI4083.1.

Goldenberg, S. B., C. W. Landsea, A. M. Mestas-Nuñez, and W. M. Gray, 2001: The recent increase in Atlantic hurricane activity: Causes and implications. *Science*, **293**, 474–479, doi:10.1126/science.1060040.

Gulev, S. K., M. Latif, N. Keenlyside, W. Park, and K. P. Koltermann, 2013: North Atlantic Ocean control on surface heat flux on multidecadal timescales. *Nature*, **499**, 464–467, doi:10.1038/nature12268.

Hoskins, B. J., and P. J. Valdes, 1990: On the existence of storm tracks. *J. Atmos. Sci.*, **47**, 1854–1864, doi:10.1175/1520-0469(1990)047<1854:OTEOST>2.0.CO;2.

Johnson, H. L., and D. Marshall, 2002: A theory for the surface Atlantic response to thermohaline variability. *J. Phys. Oceanogr.*, **32**, 1121–1132, doi:10.1175/1520-0485(2002)032<1121:ATFTSA>2.0.CO;2.

Klotzbach, P. J., 2011: The Influence of El Niño–Southern Oscillation and the Atlantic multidecadal oscillation on Caribbean tropical cyclone activity. *J. Climate*, **24**, 721–731, doi:10.1175/2010JCLI3705.1.

Knight, J. R., R. J. Allan, C. K. Folland, M. Vellinga, and M. E. Mann, 2005: A signature of persistent natural thermohaline circulation cycles in observed climate. *Geophys. Res. Lett.*, **32**, L20708, doi:10.1029/2005GL024233.

Kwon, Y.-O., and C. Frankignoul, 2012: Stochastically-driven multidecadal variability of the Atlantic meridional overturning circulation in CCSM3. *Climate Dyn.*, **38**, 859–876, doi:10.1007/s00382-011-1040-2.

——, and ——, 2014: Mechanisms of multidecadal Atlantic meridional overturning circulation variability diagnosed in depth versus density space. *J. Climate*, **27**, 9359–9376, doi:10.1175/JCLI-D-14-00228.1.

Li, Y., and N.-G. Lau, 2012: Impact of ENSO on the atmospheric variability over the North Atlantic in late winter—Role of transient eddies. *J. Climate*, **25**, 320–342, doi:10.1175/JCLI-D-11-00037.1.

Marini, C., and C. Frankignoul, 2014: An attempt to deconstruct the Atlantic Multidecadal Oscillation. *Climate Dyn.*, **43**, 607–625, doi:10.1007/s00382-013-1852-3.

Marshall, J., H. Johnson, and J. Goodman, 2001: A study of the interaction of the North Atlantic Oscillation with ocean circulation. *J. Climate*, **14**, 1399–1421, doi:10.1175/1520-0442(2001)014<1399:ASOTIO>2.0.CO;2.

Medhaug, I., and T. Furevik, 2011: North Atlantic 20th century multidecadal variability in coupled climate models: Sea surface temperature and ocean overturning circulation. *Climate Dyn.*, **7**, 389–404, doi:10.5194/os-7-389-2011.

Msadek, R., C. Frankignoul, and L. Z. X. Li, 2011: Mechanisms of the atmospheric response to North Atlantic multidecadal variability: A model study. *Climate Dyn.*, **36**, 1255–1276, doi:10.1007/s00382-010-0958-0.

Namias, J., and B. M. Born, 1970: Temporal coherence in North Pacific sea-surface temperature patterns. *J. Geophys. Res.*, **75**, 5952–5955, doi:10.1029/JC075i030p05952.

Omrani, N.-E., N. S. Keenlyside, J. Bader, and E. Manzini, 2014: Stratosphere key for wintertime atmospheric response to warm Atlantic decadal conditions. *Climate Dyn.*, **42**, 649–663, doi:10.1007/s00382-013-1860-3.

Park, S., C. Deser, and M. A. Alexander, 2005: Estimation of the surface heat flux response to sea surface temperature anomalies over the global ocean. *J. Climate*, **18**, 4582–4599, doi:10.1175/JCLI3521.1.

Peings, Y., and G. Magnusdottir, 2014: Forcing of the wintertime atmospheric circulation by the multidecadal fluctuations of the

North Atlantic Ocean. *Environ. Res. Lett.*, **9**, 034018, doi:10.1088/1748-9326/9/3/034018.

Rivière, G., 2009: Effect of latitudinal variations in low-level baroclinicity on eddy life cycles and upper-tropospheric wave-breaking processes. *J. Atmos. Sci.*, **66**, 1569–1592, doi:10.1175/2008JAS2919.1.

Rossby, T., 1996: The North Atlantic Current and surrounding waters: At the crossroads. *Rev. Geophys.*, **34**, 463–481, doi:10.1029/96RG02214.

Schneider, N., and B. D. Cornuelle, 2005: The forcing of the Pacific decadal oscillation. *J. Climate*, **18**, 4355–4373, doi:10.1175/JCLI3527.1.

Sutton, R. T., and D. L. Hodson, 2005: Atlantic Ocean forcing of North American and European summer climate. *Science*, **309**, 115–118, doi:10.1126/science.1109496.

Thompson, D. W. J., S. Lee, and M. P. Balwin, 2003: Atmospheric processes governing the Northern Hemisphere annular mode/North Atlantic Oscillation. *The North Atlantic Oscillation: Climatic Significance and Environmental Impact, Geophys. Monogr.*, Vol. 134, Amer. Geophys. Union, 81–112, doi:10.1029/134GM05.

Ting, M., Y. Kushnir, and C. Li, 2014: North Atlantic Multidecadal SST Oscillation: External forcing versus internal variability. *J. Mar. Syst.*, **133**, 27–38, doi:10.1016/j.jmarsys.2013.07.006.

Woollings, T., J. M. Gregory, J. G. Pinto, M. Reyers, and D. J. Brayshaw, 2012: Response of the North Atlantic storm track to climate change shaped by ocean–atmosphere coupling. *Nat. Geosci.*, **5**, 313–317, doi:10.1038/ngeo1438.

Yeager, S., 2015: Topographic coupling of the Atlantic overturning and gyre circulations. *J. Phys. Oceanogr.*, **45**, 1258–1284, doi:10.1175/JPO-D-14-0100.1.

——, and G. Danabasoglu, 2014: The origins of late-twentieth-century variations in the large-scale North Atlantic circulation. *J. Climate*, **27**, 3222–3247, doi:10.1175/JCLI-D-13-00125.1.

Zhang, R., 2008: Coherent surface-subsurface fingerprint of the Atlantic meridional overturning circulation. *Geophys. Res. Lett.*, **35**, L20705, doi:10.1029/2008GL035463.

——, and G. K. Vallis, 2007: The role of bottom vortex stretching on the path of the North Atlantic western boundary current and on the northern recirculation gyre. *J. Phys. Oceanogr.*, **37**, 2053–2080, doi:10.1175/JPO3102.1.